

Nonequilibrium phonon transport induced by finite sizes: Effect of phonon-phonon couplingJiaxuan Xu ^{1,*}, Yue Hu,^{1,*} Xiulin Ruan,² Xinyu Wang ³, Tianli Feng,^{4,†} and Hua Bao ^{1,‡}¹University of Michigan–Shanghai Jiao Tong University Joint Institute, Shanghai Jiao Tong University, Shanghai 200240, People’s Republic of China²School of Mechanical Engineering and the Birk Nanotechnology Center, Purdue University, West Lafayette, Indiana 47907-2088, USA³Institute of Thermal Science and Technology, Shandong University, Jinan 250061, People’s Republic of China⁴Department of Mechanical Engineering, University of Utah, Salt Lake City, Utah 84112, USA

(Received 15 June 2021; revised 1 September 2021; accepted 2 September 2021; published 23 September 2021)

In heat conduction through a homogenous nanomaterial, various phonons may exhibit diverse temperatures even at the same location at a steady state, known as the local phonon nonequilibrium phenomenon. Different phonons are often considered to behave independently, and the phonons with longer mean free paths (MFPs) have smaller temperature gradients. That is, the temperature gradient exhibits the following order: ballistic phonons < semiballistic phonons \approx lattice (average) temperature gradient < diffusive phonons, where ballistic phonons have MFPs much larger than the characteristic length, semiballistic phonons have MFPs like the characteristic length, and diffusive phonons have MFPs much smaller than the characteristic length. However, in this paper, we reveal that the effect of phonon-phonon coupling leads nonequilibrium phonon temperature gradients to the following trend: diffusive phonon temperature gradients will decrease to the lattice temperature, and temperature gradients of some semiballistic phonons even surpass that of diffusive phonons. The diffusive phonon temperature is merged onto the lattice temperature since they have large scattering rates and can be equilibrated quickly to the lattice temperature after traveling for a short distance away from the boundaries into the nanomaterial. The semiballistic phonons have large scattering rates but not large enough to bring them down to the lattice temperature. To obtain a further understanding of the nonequilibrium phonon temperatures, we have also derived a simple analytical model which can accurately predict the temperature profiles of all individual phonons given their MFPs. Using this model, we find that, near the boundary, phonon temperatures decay with position exponentially (instead of linearly), with a rate inversely proportional to their MFPs. Our findings offer insight for the understanding and prediction of phonon nonequilibrium temperatures within nanodevices.

DOI: [10.1103/PhysRevB.104.104310](https://doi.org/10.1103/PhysRevB.104.104310)**I. INTRODUCTION**

Nanoscale thermal transport driven by phonons has been of great interest in recent decades [1–8] due to its unique characteristics compared with conventional Fourier thermal transport. In Fourier thermal transport, a single linear temperature profile is built between the hot and cold ends of a device at a steady state. However, when heat flows through a nanodevice from the hot end to the cold end at a steady state, various phonons may exhibit diverse temperatures even at the same location, which is called the *size effect-induced phonon temperature nonequilibrium* [9–11]. Ballistic phonons [mean free path (MFP) \gg device length] can transport through the device without much loss of energy due to the absence of phonon-phonon scattering. As a result, their temperature profiles are nearly flat, with a nearly zero temperature gradient, being very different from the nonzero average temperature gradient through the device. The other phonons, which have MFPs similar to or even smaller than the device length, have a

nonzero temperature gradient, which can be even greater than the average temperature gradient. Therefore, various phonons have various temperatures even at the same location. This is called *modal phonon temperature nonequilibrium* [12–14]. Authors of recent studies have found that understanding the nonequilibrium thermal transport is significant for the performance of many applications such as nanomaterial thermal property measurements [15–17], electronic devices [18–20], and ultrafast laser processing [21,22].

Many studies have been conducted to resolve the nonequilibrium phonon temperature using various methods, including the Raman spectroscopy experiments [15–17,23], multitemperature model [12,13], molecular dynamics (MD) simulations [24–26], and phonon Boltzmann transport equation (BTE) simulations [21,27–33]. The Raman spectroscopy experiments are conducted near the diffusive regime (the sample size is much larger than the phonon MFP) and can resolve some individual zone-center optical phonon temperatures [15]. The multitemperature model can resolve nonequilibrium among different phonon modes but neglects the effect of ballistic transport [12]. MD simulations are conducted at a relatively small scale (far from the diffusive regime) [8]. In comparison, only the phonon BTE can cover the entire ballistic-to-diffusive regime and obtain detailed phonon temperatures for further analysis [28,31,32]. However, only a few

*These authors contributed equally to this work.

†tianli.feng@utah.edu

‡hua.bao@sjtu.edu.cn

analyses of the nonequilibrium phonon temperature based on the phonon BTE have been conducted. Recently, by studying the detailed information obtained from the simplified phonon BTE (the McKelvey-Shockley flux method), Maassen and Lundstrom [31] found a one-to-one correspondence between the phonon MFP and the nonequilibrium phonon temperature. For cross-plane heat conduction in thin films, the nonequilibrium phonon temperature gradient monotonically increases with the decreasing phonon MFP. This correspondence not only helps to understand the nonequilibrium thermal transport but can also be used for MFP spectroscopy which has received much attention recently [34–36]. However, their conclusions are built on the assumption that phonons with various MFPs transport independently through the device. Since the effect of phonon-phonon coupling is ignored, it may lead to insufficient understanding of the nonequilibrium phonon temperature.

In this paper, we employ the mode-resolved phonon BTE to calculate the modal phonon temperatures. As a representative nanoscale heat conduction problem, the cross-plane heat conduction through silicon thin films is taken as the study case. The effect of phonon-phonon coupling is included in the mode-resolved phonon BTE, which shows significant differences in phonon temperature profile in comparison with the case without coupling. To further understand the nonequilibrium phonon temperatures, an analytical expression is derived for the nonequilibrium phonon temperature. Furthermore, we also modify the one-to-one correspondence, i.e., the mapping from the phonon MFP spectra to the nonequilibrium phonon temperature, which can be used to reconstruct the MFP distribution from the phonon temperature.

II. NONEQUILIBRIUM PHONON TEMPERATURES

Local phonon temperature is a representation of phonon energy density at a location [6,26,37]. Different levels of resolution of the nonequilibrium phonon temperature have been used previously [12,15,26,37]. The first level is the branch-level phonon temperature, which is the average temperature of all phonons in the same branch j [12]. The second level is the MFP-resolved phonon temperature, i.e., the average temperature of all phonon modes in various transport directions with the same MFP [37]. The third level is the modal phonon temperature, which is the average temperature of two phonon modes with specific wave vector \mathbf{q} and $-\mathbf{q}$ and the same branch j [26]. The two phonon modes have the same MFP and opposite propagation directions. As the third level provides the most detailed information of heat transfer [26], we use it in this paper, i.e., T_λ , where λ represents two phonon modes with specific wave vector \mathbf{q} and $-\mathbf{q}$ and the same branch j .

To study the mode-resolved phonon temperatures, we employ the mode-resolved phonon BTE with the relaxation time approximation, which is valid for silicon [8]. Authors of previous studies adopted a simplified phonon BTE (the McKelvey-Shockley flux method) [30,31], which divides the phonons into forward- and reverse-moving streams and assumes that phonons with the same MFP in each stream have the same temperature. They excluded the effect of phonon-phonon coupling by assuming that phonons with different MFPs have different equilibrium Bose-Einstein statistics relying on their temperatures and are independent on each

other. In our mode-resolved phonon BTE, all phonons interact with common equilibrium Bose-Einstein statistics (characterized as the lattice temperature), which thus includes the coupling among all phonon modes. Recently, Abarbanel and Maassen [38] and Maassen and Askarpour [39] extended the McKelvey-Shockley flux method to include the effect of phonon-phonon coupling. This method has smaller computational costs than numerically solving the phonon BTE, but the accuracy in the ballistic regime is also lower.

The mode-resolved phonon temperatures are calculated by numerically solving the mode-resolved phonon BTE using a finite volume method (FVM) [33,40]. The numerical treatment of the mode-resolved phonon BTE is shown in Appendix A. The inputs of the mode-resolved phonon BTE including phonon capacity, group velocity, and relaxation time are obtained from the first-principles calculations [41,42]. We have sampled various phonon modes with a total of 400 different “effective” MFP values, which are the MFP (group velocity multiplies relaxation time) components in the transport direction. The two boundaries of the films are applied by thermalizing boundary conditions [8], which emit equilibrium phonons at $T_1 = 310$ K and $T_2 = 290$ K, respectively. Here, we categorize the phonon modes into three categories: (1) ballistic modes, which have large MFP $\gg L$; (2) semiballistic modes, which have moderate MFP $\sim L$; and (3) diffusive modes, which have small MFP $\ll L$.

Taking a 20-nm-thick silicon thin film as an example, we obtained the mode-resolved phonon temperatures through the film in the cases of excluding and including the phonon-phonon coupling. The results for the two cases are shown in Figs. 1(a) and 1(b), respectively. To more clearly show the difference between the two cases, we only pick three representative phonon modes in the three phonon categories, which have MFP of 100, 5, and 1 nm, representing ballistic, semiballistic, and diffusive phonon modes, respectively. We also include the lattice temperature (T_L) for both cases as a guideline. Both cases (with and without the phonon-phonon coupling) show some common characteristics. First, they both predict large local nonequilibrium phonon temperatures, i.e., different phonon modes have different temperatures at the same location, being consistent with the MD simulation results [26]. Second, in both cases, the temperature of the ballistic phonon deviates the most from the lattice temperature and has a nearly flat profile, i.e., a small temperature gradient. Third, the temperature at the boundary (on the hot side) of each phonon mode increases monotonically with decreasing MFP, i.e., phonons that are more diffusive have larger temperatures on the hot side and lower temperatures on the cold side. Last, the two cases give similar lattice temperatures.

Meanwhile, the two cases exhibit key differences, which are described as follows. The case without the phonon-phonon coupling [Fig. 1(a)] shows that the phonon temperature gradient increases monotonically with decreasing MFP, i.e., the temperature gradients have the order $\nabla T_{\text{diffusive}} > \nabla T_{\text{semiballistic}} \sim \nabla T_L > \nabla T_{\text{ballistic}}$. This is because the phonons that are more ballistic have longer MFPs and less collision or energy loss after traveling for a given distance. For example, the ballistic mode with MFP = 100 nm will have only 0.2 collisions (on average) during the travel through the 20-nm-thick silicon film, and its energy loss is small, and equivalently,

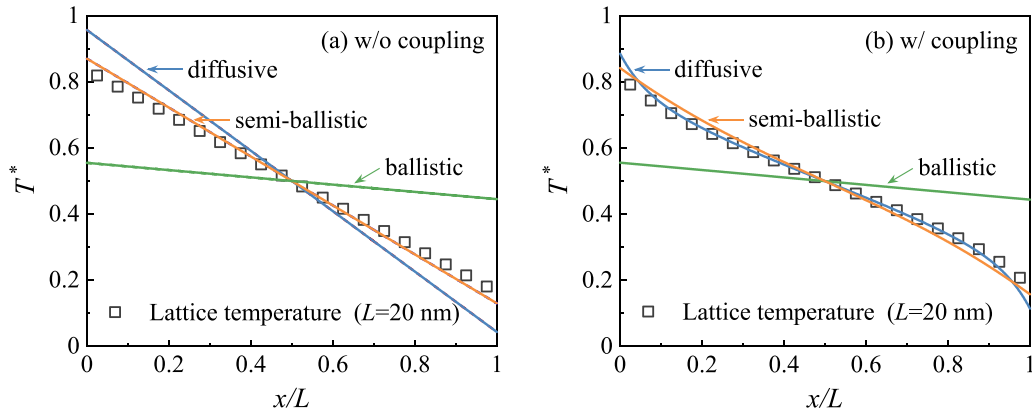


FIG. 1. The dimensionless phonon temperature $T^* = (T_\lambda - T_2)/(T_1 - T_2)$ for silicon thin film ($L = 20$ nm) vs dimensionless position x/L for the cases (a) without and (b) with the phonon-phonon coupling effect.

the temperature gradient is small. In contrast, the modes with $MFP = 5$ and 1 nm will have 4 and 20 collisions during the travel, respectively. As a result, their temperature gradients are large. This analysis was done based on the assumption that those phonon modes with different MFPs do not interact with each other [30,31].

However, after including the phonon-phonon coupling [Fig. 1(b)], we find that the phonon temperature gradient does not increase monotonically with decreasing MFP. It is the semiballistic mode rather than the diffusive mode that shows the largest temperature gradient [30,31]. As shown

in Fig. 1(b), the order of temperature gradients becomes $\nabla T_{\text{semiballistic}} > \nabla T_{\text{diffusive}} = \nabla T_L > \nabla T_{\text{ballistic}}$. The temperature of the diffusive mode overlaps with T_L quickly after it is emitted from the thermal boundaries. This is understandable since diffusive phonons have frequent collisions with other modes, and their temperatures can be quickly equilibrated with the lattice temperature after traveling for a few MFPs. In the case shown in Fig. 1(b), the diffusive mode has a $MFP = 1$ nm, and its temperature merges onto the lattice temperature at $\sim 2\text{--}3$ nm away from the boundaries. The semiballistic mode in Fig. 1(b) has a larger temperature at the boundary

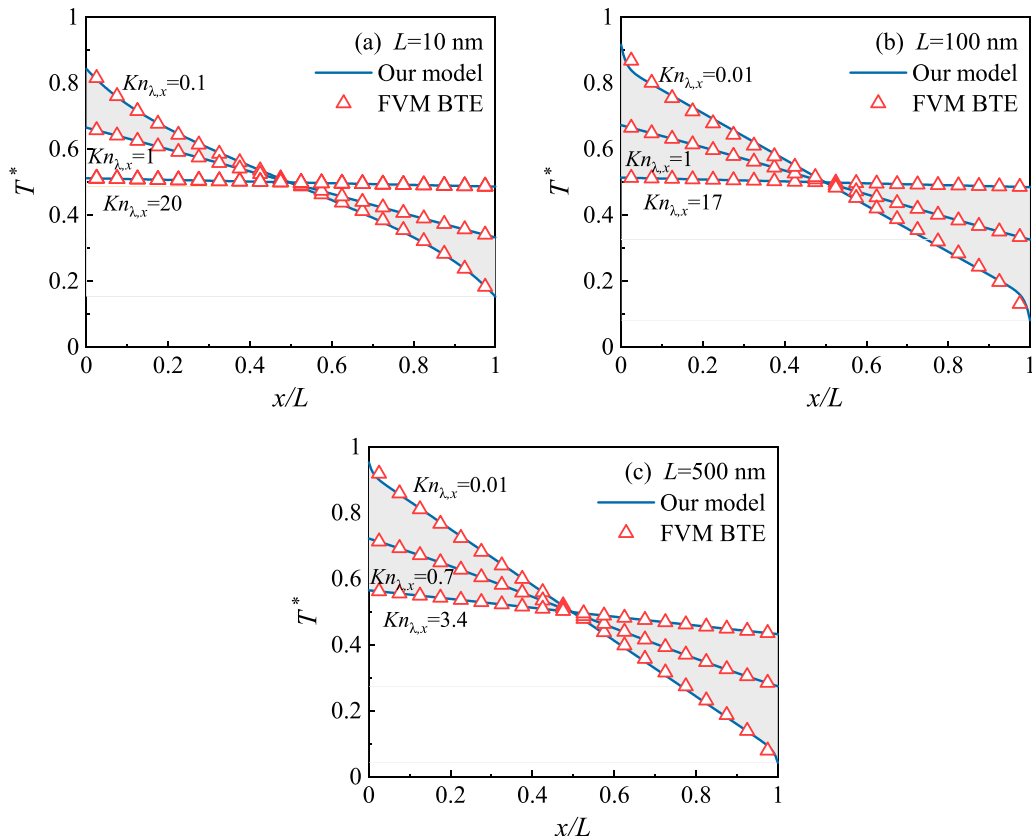


FIG. 2. Selected nonequilibrium phonon temperatures for the validation of our analytical model on silicon thin film with a thickness (a) $L = 10$ nm, (b) $L = 100$ nm, and (c) $L = 500$ nm. The gray shaded regions represent the temperatures of other phonon modes.

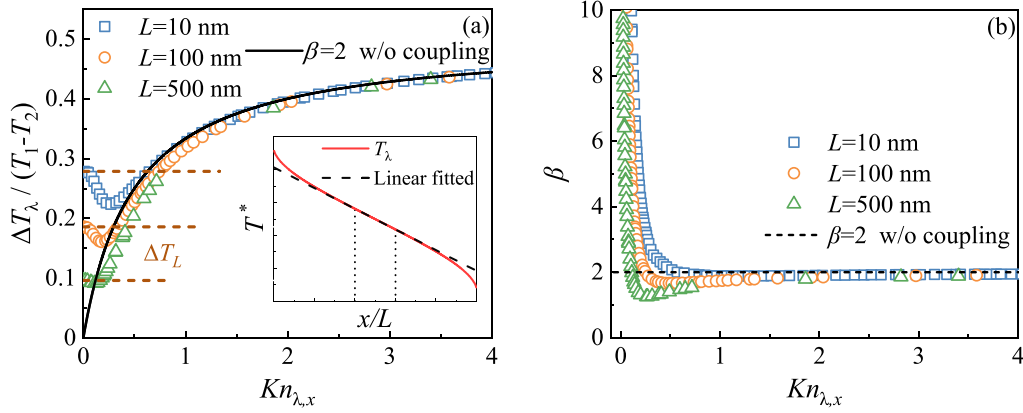


FIG. 3. (a) The dimensionless phonon temperature jumps at the boundary $\Delta T_\lambda / (T_1 - T_2)$ vs the mode-level Knudsen number $Kn_{\lambda,x} = \Lambda_{\lambda,x} / L$ for film thicknesses $L = 10, 100,$ and 500 nm. The inset of (a) shows that the ΔT_λ is extracted by linear fitting of the central part of the temperature profile. (b) The correspondence coefficient β between the nonequilibrium phonon temperature and phonon mean free path (MFP) spectra vs the Knudsen number $Kn_{\lambda,x}$.

than T_L (on the hot side), and its temperature also tends to merge onto T_L after it is emitted from the boundaries. However, collisions of semiballistic phonons with other phonon modes are not frequent enough for them to merge onto T_L as the diffusive mode does. As a result, the temperature gradient of the semiballistic mode is larger than ∇T_L . In contrast to the diffusive and semiballistic modes, the ballistic modes have even fewer collisions and still behave similarly to the case without the coupling because those modes do not have strong phonon-phonon coupling. Overall, the average of $\nabla T_{\text{ballistic}}$, $\nabla T_{\text{semiballistic}}$, and $\nabla T_{\text{diffusive}}$ of all the hundreds of phonon modes is equal to ∇T_L . Our phonon BTE has been verified by the nonequilibrium MD [8]. It is also exciting to compare the simulation results with experiments when experimental techniques are available in the future.

III. ANALYTICAL MODEL FOR PHONON TEMPERATURE PROFILES

To further understand and quantitatively predict the phonon nonequilibrium temperatures in a simple way instead of solving the complicated mode-resolved BTE numerically, we derived an analytical model for the nonequilibrium phonon temperatures by assuming that the lattice temperature T_L is linear and known (see Appendix B for the details of derivation). The modal phonon temperature can be written as

$$T_\lambda = T_L + \frac{1}{2} \left[A \exp\left(-\frac{x}{\Lambda_{\lambda,x}}\right) + B \exp\left(\frac{x-L}{\Lambda_{\lambda,x}}\right) \right], \quad (1)$$

where $A = T_1 - b + a\Lambda_{\lambda,x}$ and $B = T_2 - b - aL - a\Lambda_{\lambda,x}$ with a and b determined by the lattice temperature $T_L = ax + b$. Here, $\Lambda_{\lambda,x}$ is the phonon MFP component projection along the temperature gradient direction. The lattice temperature T_L can be obtained by the semi-analytical solution in the work of Hua and Minnich [29], MD simulations [43], or directly from experiments [44]. To validate our analytical model, we compare the results predicted by the present model with those obtained from the numerically solved BTE. The lattice temperature is extracted from the numerical results, and the

MFPs of the phonon modes are the same as those used in the numerical solver. In Fig. 2, we present results for silicon films with three thicknesses ($L = 10, 100,$ and 500 nm) and three selected phonon temperatures (including the temperature with the largest gradient and smallest gradient) for each thickness. The shaded regions in Fig. 2 represent the temperatures of other phonons. Good agreement is achieved for all phonon modes in all three films.

Equation (1) shows that the nonequilibrium phonon temperature equals the lattice temperature plus an exponential term $A \exp(-x/\Lambda_{\lambda,x}) + B \exp((x-L)/\Lambda_{\lambda,x})$. This exponential term decays when phonons travel away from boundaries, and the decay rate is $1/\Lambda_{\lambda,x}$. This is because the physical origin of decay is the phonon-phonon scattering, namely, the coupling effect. Figure 1 shows a trend of diffusive phonon temperatures decaying to the lattice temperature near the boundaries, which is consistent with Eq. (1). For diffusive phonons, the exponential term $A \exp(-x/\Lambda_{\lambda,x}) + B \exp((x-L)/\Lambda_{\lambda,x})$ quickly decays to zero due to the small phonon MFP. Thus, the diffusive phonon temperatures quickly decay to the lattice temperature, which leads to a lower temperature gradient than the semiballistic phonon temperatures, as shown in Fig. 1. The rapid temperature decay also indicates that the diffusive phonons are strongly coupled with other phonons. As the phonon MFP increases, the exponential term becomes dominant and slowly decays due to the weak coupling effect, causing the phonon temperature to become almost linear, like the phonon temperature without coupling. For ballistic phonons, the large phonon MFP causes the phonon temperature to be reduced to $T_\lambda = aL/2 + b$ at the Casimir limit [9].

IV. REVISED MODEL FOR PHONON TEMPERATURE GRADIENTS

It is of great interest to predict temperature gradients of phonons using their MFPs. Assuming there is no phonon-phonon coupling effect, Maassen and Lundstrom [31] have developed the following equation for model temperature

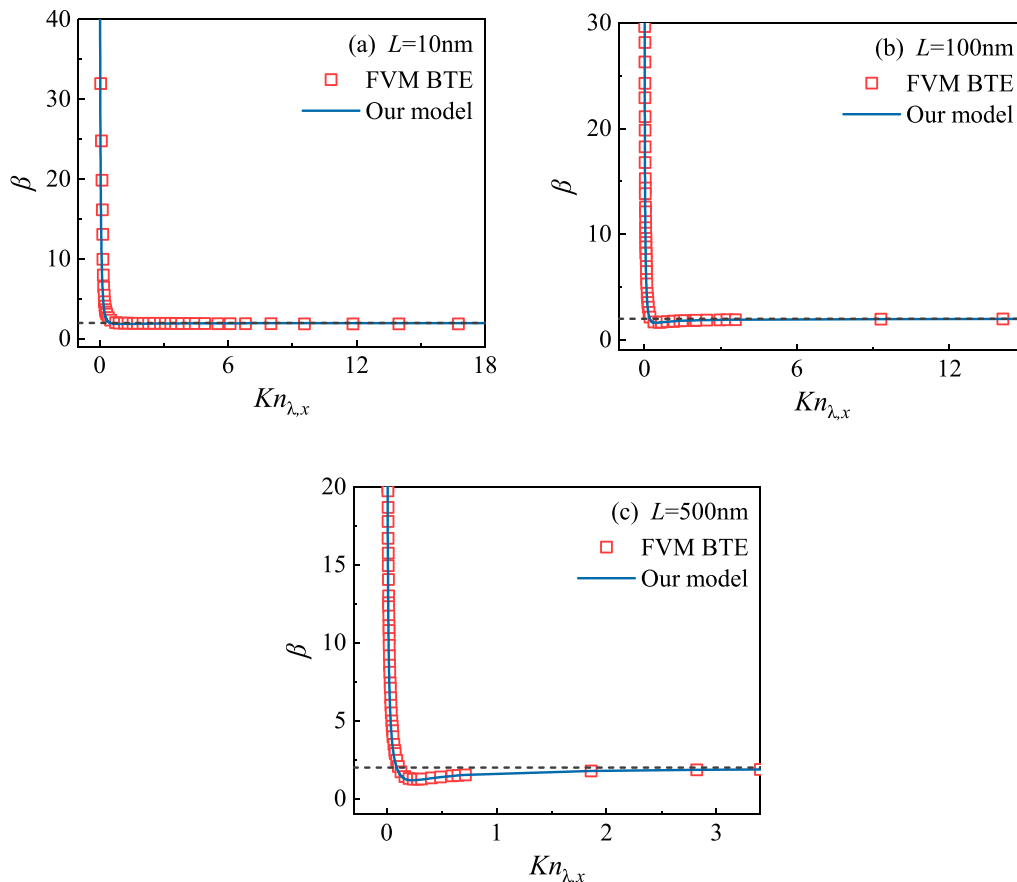


FIG. 4. Comparison of the correspondence coefficient β between our analytical model and the finite volume method (FVM) Boltzmann transport equation (BTE) results for (a) $L = 10$ nm, (b) $L = 100$ nm, and (c) $L = 500$ nm. The dashed lines represent $\beta = 2$, i.e., without the phonon-phonon coupling effect.

distribution:

$$\frac{T_1 - T_2}{2\Delta T_\lambda} = 1 + \frac{1}{\beta Kn_{\lambda,x}}, \quad (2)$$

where $Kn_{\lambda,x}$ is the Knudsen number and is equal to $\Lambda_{\lambda,x}/L$. Here, ΔT_λ is the phonon temperature jump at boundaries. The coefficient $\beta = 2$ is a constant for all phonons [31,45]. This indicates that the phonon temperature jumps increase monotonically with MFPs, as already shown in Fig. 1(a). Based on this, the inverse mapping can be adopted to reconstruct the phonon MFP distribution from the nonequilibrium temperature [26]. However, based on the discussions above, the mapping needs to be corrected due to the significant phonon-phonon coupling effect.

Figure 3(a) shows the dimensionless phonon temperature jumps $\Delta T_\lambda/(T_1 - T_2)$ vs the modal Knudsen number $Kn_{\lambda,x}$ for films with thicknesses $L = 10$, 100, and 500 nm (symbols) when considering the phonon-phonon coupling. The phonon temperature jumps are extracted by linearly fitting the central part of the phonon temperature (x/L from 0.4 to 0.6), as shown in the inset of Fig. 3(a). Meanwhile, the predicted phonon temperature jumps without considering the coupling (i.e., from Eq. (2) with $\beta = 2$) is also plotted

as the black solid curve in Fig. 3(a). The phonon temperature jumps without coupling approach zero for diffusive phonons and monotonically increase as the phonon transport becomes more ballistic until it reaches the Casimir limit [9]. When considering the phonon-phonon coupling effect, ΔT_λ of the ballistic phonons remains close to the values without coupling due to a weak coupling effect. However, in the diffusive regime, ΔT_λ for these three films all obviously deviate from the values without coupling and increase back to the lattice temperature jumps [as shown by the brown dashed lines in Fig. 3(a)] because of the strong coupling with other phonons.

The correspondence coefficient β is also affected by the phonon-phonon coupling [Fig. 3(b)]. Instead of a constant, the correspondence coefficient β remains ~ 2 for ballistic phonons and sharply increases for diffusive phonons. The reason is that ΔT_λ of diffusive phonons approaches a constant corresponding to the lattice temperature jump at the boundary, as shown in Fig. 3(a). For different film thicknesses, the trends of ΔT_λ and β are similar, which all converge to the values without coupling in the ballistic transport regime and deviate from it in the diffusive transport regime. Based on the analytical expression of the nonequilibrium phonon temperature [Eq. (1)], we can derive a quantitative description

of the correspondence coefficient β :

$$\beta = \frac{1}{Kn_{\lambda,x}} \frac{T_1 - T_2 + aL - \frac{5}{2}(A - B) \left[\exp\left(\frac{-2}{5Kn_{\lambda,x}}\right) - \exp\left(\frac{-3}{5Kn_{\lambda,x}}\right) \right]}{-aL + \frac{5}{2}(A - B) \left[\exp\left(\frac{-2}{5Kn_{\lambda,x}}\right) - \exp\left(\frac{-3}{5Kn_{\lambda,x}}\right) \right]}. \quad (3)$$

The parameters $A = T_1 - b + a\Lambda_{\lambda,x}$ and $B = T_2 - b - aL - a\Lambda_{\lambda,x}$ are determined by the lattice temperature and the phonon MFP. As shown in Fig. 4, the results from this analytical expression Eq. (3) (solid lines) agree well with that of the FVM BTE results (square symbols). This indicates that our analytical model provides the correct and quantitative mapping from the phonon MFP spectra to the nonequilibrium phonon temperature.

The inverse process of this mapping (from the nonequilibrium phonon temperature to the phonon MFP spectra) can be applied to the MFP spectroscopy [26]. The corrected correspondence coefficient β from our analytical model can be used to accurately reconstruct the phonon MFP distribution.

V. SUMMARY AND CONCLUSIONS

In summary, we have studied the modal nonequilibrium phonon temperatures across thin films based on the mode-resolved phonon BTE. Considering the effect of phonon-phonon coupling, we find that the phonon temperature gradients do not increase monotonically with decreasing phonon MFP as understood in the literature, i.e., $\nabla T_{\text{ballistic}} < \nabla T_{\text{semiballistic}} \sim \nabla T_L < \nabla T_{\text{diffusive}}$. Instead, phonon temperature gradients still increase with decreasing MFP in the ballistic regime but reach the maxima in the semiballistic regime and then decrease to the lattice temperature in diffusive regime due to the strong phonon-phonon coupling. A simple analytical model is derived to predict the modal phonon temperature gradient ∇T_λ based on the phonon MFP $\Lambda_{\lambda,x}$ with similar accuracy as solving the complicated mode-resolved BTE numerically. Our analytical model shows that the phonon temperature exponentially decays to the lattice temperature from the boundaries. The different decay rates cause the nonequilibrium thermal transport and represent the strength of the coupling with other phonons. Our analytical model also provides the correct mapping from the nonequilibrium phonon temperature to the phonon MFP spectra. The inverse mapping can be applied to the MFP spectroscopy, i.e., reconstructing the phonon MFP distribution from the phonon temperature. This paper provides significant insight into nanoscale thermal transport through crystalline materials and will have a great impact on the study of thermal management of electronics.

ACKNOWLEDGMENTS

J.X., Y.H., and H.B. acknowledge the support by the National Natural Science Foundation of China (Grant No. 52122606). Simulations were performed on the π 2.0 cluster supported by the Center for High Performance Computing at Shanghai Jiao Tong University.

APPENDIX A: THE MODE-RESOLVED PHONON BTE AND NUMERICAL TREATMENT

The steady-state mode-resolved phonon BTE [19,27,37,40] is given by

$$\mathbf{v}_\lambda \cdot \nabla e_\lambda = \left(\frac{\partial e_\lambda}{\partial t} \right)_{\text{scatter}}, \quad (A1)$$

where e_λ is the phonon energy distribution function. Here, \mathbf{v}_λ is the group velocity of phonon modes, which is assumed to be isotropic. Also, $(\partial e_\lambda / \partial t)_{\text{scatter}}$ is the phonon scattering term [6]. The subscript λ in the main text and appendixes represents two phonon modes with specific wave vector \mathbf{q} and $-\mathbf{q}$ and the same branch j . Due to the complexity of the rigorous form, the scattering term of the BTE is commonly simplified by the relaxation time approximation, which is valid for silicon [37]:

$$\mathbf{v}_\lambda \cdot \nabla e_\lambda = \left(\frac{e_\lambda - e_\lambda^0}{\tau_\lambda} \right), \quad (A2)$$

where τ_λ is the relaxation time which is the average time between two subsequent phonon-phonon collisions and is a measure of the time required for a nonequilibrium system to relax to an equilibrium state [1]. Here, e_λ^0 in Eq. (A2) is the phonon energy density at the equilibrium state characterized by the lattice temperature T_L ($T_L = 4\pi e_\lambda^0 / C_\lambda$), i.e., the common equilibrium temperature that all phonon modes are coupled with. For circumstances without coupling, equilibrium states of phonons with different MFPs are characterized by different temperatures and are independent of each other. According to the energy conservation rule [37], the integration of the scattering term over the angular space and phonon frequency should be zero, i.e.,

$$\int_{4\pi} \sum_p \int_{\omega_{\min}}^{\omega_{\max}} \frac{e_\lambda^0 - e_\lambda}{\tau_\lambda} d\omega d\Omega = 0. \quad (A3)$$

Equation (A3) illustrates the relation between e_λ^0 and the modal phonon energy distribution e_λ . Thus, after solving the BTE and obtaining the e_λ , we can calculate the lattice temperature T_L ($T_L = 4\pi e_\lambda^0 / C_\lambda$) from

$$T_L = \frac{\int_{4\pi} \sum_p \int_{\omega_{\min}}^{\omega_{\max}} \frac{e_\lambda}{\tau_\lambda} d\omega d\Omega}{\sum_p \int_{\omega_{\min}}^{\omega_{\max}} \frac{C_\lambda}{\tau_\lambda} d\omega}. \quad (A4)$$

The properties \mathbf{v}_λ , C_λ , and τ_λ of each phonon mode are obtained from the first-principles calculations and are taken as inputs to solve the phonon BTE. Phonon group velocity \mathbf{v}_λ and heat capacity C_λ are calculated from the harmonic lattice dynamics using second-order interatomic force constants (IFCs) in QUANTUM ESPRESSO, and the relaxation time τ_λ is calculated from the anharmonic lattice dynamics which takes both second- and third-order IFCs and applies the single mode relaxation time approximation method to calculate the phonon

scattering rate in SHENGBTE [46]. Only three-phonon scattering processes are considered in our calculation. We use $30 \times 30 \times 30$ q points to sample the Brillouin zone. Details of the first-principles calculations can be found in Refs. [6,41,42].

After obtaining the inputs, we use the deterministic solution to solve the mode-resolved phonon BTE in this paper. For numerically solving the mode-resolved phonon BTE, it is not necessary to sample all phonon modes in first-principles calculations [37]. We divided the phonon MFP spectra into 100 phonon bands based on a convergence test. We applied the discrete ordinates method to divide the angular space, and the FVM is adopted for spatial discretization [33,37]. We use 16 angles and 1000 cells in our calculations based on a convergence test. Further detailed numerical methods for solving the phonon BTE can be found in previous studies [19,27,37,40].

APPENDIX B: THE ANALYTICAL MODEL

We start with the steady-state mode-resolved phonon BTE with the energy form under the relaxation time approximation for a one-dimensional cross-plane problem:

$$v_x \frac{\partial e_\lambda}{\partial x} = \frac{e_\lambda^0(T_L) - e_\lambda}{\tau_\lambda}, \quad (\text{B1})$$

where v_x is the projection of the group velocity \mathbf{v}_λ along the cross-plane direction. Since Eq. (B1) is a first-order inhomogeneous differential equation, the general solution is

$$e_\lambda = \left[\phi + \frac{1}{4\pi} \frac{C_\lambda}{\Lambda_{\lambda,x}} \int T_L \exp\left(\frac{|x - x_B|}{\Lambda_{\lambda,x}}\right) dx \right] \times \exp\left(-\frac{|x - x_B|}{\Lambda_{\lambda,x}}\right), \quad (\text{B2})$$

where $\Lambda_{\lambda,x}$ is the phonon MFP component projection along the cross-plane direction. Here, x_B is the location of the boundary. Also, ϕ is determined by the thermalizing bound-

aries conditions:

$$\begin{aligned} e_\lambda(x=0) &= e_\lambda^0(T_1), \\ e_\lambda(x=L) &= e_\lambda^0(T_2). \end{aligned} \quad (\text{B3})$$

Then the temperature of the phonon mode is given by $T_\lambda = 4\pi e_\lambda / C_\lambda$.

We define the direction of phonon transport from the hot end to the cold end as positive and the opposite as negative. Thus, we average the temperature of phonon modes with the corresponding positive and negative directions, i.e., with wave vectors \mathbf{q} and $-\mathbf{q}$, which gives the modal phonon temperature as

$$T_\lambda = \frac{1}{2} \left\{ \left[\frac{4\pi\phi_0}{C_\lambda} + \frac{1}{\Lambda_{\lambda,x}} \int T_L \exp\left(\frac{x}{\Lambda_{\lambda,x}}\right) dx \right] \exp\left(\frac{-x}{\Lambda_{\lambda,x}}\right) + \left[\frac{4\pi\phi_L}{C_\lambda} - \frac{1}{\Lambda_{\lambda,x}} \int T_L \exp\left(\frac{L-x}{\Lambda_{\lambda,x}}\right) dx \right] \exp\left(\frac{x-L}{\Lambda_{\lambda,x}}\right) \right\}. \quad (\text{B4})$$

Then we linear fit the lattice temperature distribution and simplify it into $T_L = ax + b$. This simplification is reasonable since it is the temperature gradient that we care about. Thus, applying $T_L = ax + b$ to the boundary conditions, we obtain

$$\begin{aligned} \phi_0 &= \frac{C_\lambda}{4\pi} (T_1 - b + a\Lambda_{\lambda,x}), \\ \phi_L &= \frac{C_\lambda}{4\pi} (T_2 - b - aL - a\Lambda_{\lambda,x}). \end{aligned} \quad (\text{B5})$$

Therefore, the modal phonon temperature is reduced to

$$T_\lambda = ax + b + \frac{1}{2} \left[A \exp\left(\frac{-x}{\Lambda_{\lambda,x}}\right) + B \exp\left(\frac{x-L}{\Lambda_{\lambda,x}}\right) \right], \quad (\text{B6})$$

where $A = T_1 - b + a\Lambda_{\lambda,x}$ and $B = T_2 - b - aL - a\Lambda_{\lambda,x}$.

-
- [1] G. Chen, *Nanoscale Energy Transport and Conversion: A Parallel Treatment of Electrons, Molecules, Phonons, and Photons* (Oxford University Press, Oxford, 2005).
- [2] L. A. Jauregui *et al.*, *ECS Trans.* **28**, 73 (2010).
- [3] W. G. Ma, H. D. Wang, X. Zhang, and W. Wang, *J. Appl. Phys.* **108**, 064308 (2010).
- [4] M. Hu and D. Poulikakos, *Nano Lett.* **12**, 5487 (2012).
- [5] N. Yang, X. Xu, G. Zhang, and B. Li, *AIP Advances* **2**, 041410 (2012).
- [6] H. Bao, J. Chen, X. Gu, and B.-Y. Cao, *ES Energy & Environ.* **1**, 16 (2018).
- [7] Y. Hua, H. Li, and B. Cao, *IEEE Trans. Electron Devices* **66**, 3296 (2019).
- [8] Y. Hu, T. Feng, X. Gu, Z. Fan, X. Wang, M. Lundstrom, S. S. Shrestha, and H. Bao, *Phys. Rev. B* **101**, 155308 (2020).
- [9] A. Majumdar, *J. Heat Transfer* **115**, 7 (1993).
- [10] D. P. Sellan, E. S. Landry, J. E. Turney, and A. J. H. McGaughey, and C. H. Amon, *Phys. Rev. B* **81**, 214305 (2010).
- [11] K. M. Hoogeboom-Pot *et al.*, *Proc. Natl. Acad. Sci. USA* **112**, 4846 (2015).
- [12] A. K. Vallabhaneni, D. Singh, H. Bao, J. Murthy, and X. Ruan, *Phys. Rev. B* **93**, 125432 (2016).
- [13] Z. Lu, A. Vallabhaneni, B. Cao, and X. Ruan, *Phys. Rev. B* **98**, 134309 (2018).
- [14] Z. Lu, J. Shi, and X. Ruan, *J. Appl. Phys.* **125**, 085107 (2019).
- [15] S. Sullivan, A. Vallabhaneni, I. Kholmanov, X. Ruan, J. Murthy, and L. Shi, *Nano Lett.* **17**, 2049 (2017).
- [16] R. Wang, T. Wang, H. Zobeiri, P. Yuan, C. Deng, Y. Yue, S. Xu, and X. Wang, *Nanoscale* **10**, 23087 (2018).
- [17] R. Wang, H. Zobeiri, Y. Xie, X. Wang, X. Zhang, and Y. Yue, *Adv. Sci.* **7**, 2000097 (2020).
- [18] E. Pop, R. W. Dutton, and K. E. Goodson, *Appl. Phys. Lett.* **86**, 082101 (2005).
- [19] S. V. J. Narumanchi, J. Y. Murthy, and C. H. Amon, *Heat Mass Transf.* **42**, 478 (2006).
- [20] Q. Hao, H. Zhao, and Y. Xiao, *J. Appl. Phys.* **121**, 204501 (2017).
- [21] S. Sadasivam, M. K. Y. Chan, and P. Darancet, *Phys. Rev. Lett.* **119**, 136602 (2017).
- [22] C. Ferrante *et al.*, *Nat. Commun.* **9**, 308 (2018).

- [23] H. Zobeiri, R. Wang, T. Wang, H. Lin, C. Deng, and X. Wang, *Int. J. Heat Mass Transfer* **133**, 1074 (2019).
- [24] X. Wu and T. Luo, *J. Appl. Phys.* **115**, 014901 (2014).
- [25] M. An, Q. Song, X. Yu, H. Meng, D. Ma, R. Li, Z. Jin, B. Huang, and N. Yang, *Nano Lett.* **17**, 5805 (2017).
- [26] T. Feng, W. Yao, Z. Wang, J. Shi, C. Li, B. Cao, and X. Ruan, *Phys. Rev. B* **95**, 195202 (2017).
- [27] S. Mazumder and A. Majumdar, *J. Heat Transfer* **123**, 749 (2001).
- [28] D. Singh, J. Y. Murthy, and T. S. Fisher, *J. Heat Transfer* **133**, 122401 (2011).
- [29] C. Hua and A. J. Minnich, *J. Appl. Phys.* **117**, 175306 (2015).
- [30] J. Maassen and M. Lundstrom, *J. Appl. Phys.* **117**, 135102 (2015).
- [31] J. Maassen and M. Lundstrom, *J. Appl. Phys.* **117**, 035104 (2015).
- [32] J. Kaiser, T. Feng, J. Maassen, X. Wang, X. Ruan, and M. Lundstrom, *J. Appl. Phys.* **121**, 044302 (2017).
- [33] S. Zahiri, J. Zuo, Y. Shen, and H. Bao, *Appl. Therm. Eng.* **141**, 126 (2018).
- [34] A. J. Minnich, J. A. Johnson, A. J. Schmidt, K. Esfarjani, M. S. Dresselhaus, K. A. Nelson, and G. Chen, *Phys. Rev. Lett.* **107**, 095901 (2011).
- [35] A. J. Minnich, *Phys. Rev. Lett.* **109**, 205901 (2012).
- [36] Y. Hu, L. Zeng, A. J. Minnich, M. S. Dresselhaus, and G. Chen, *Nat. Nanotechnol.* **10**, 701 (2015).
- [37] J. M. Loy, J. Y. Murthy, and D. Singh, *J. Heat Transfer* **135**, 011008 (2012).
- [38] D. Abarbanel and J. Maassen, *J. Appl. Phys.* **121**, 204305 (2017).
- [39] J. Maassen and V. Askarpour, *APL Mater.* **7**, 013203 (2018).
- [40] J. Y. Murthy and S. R. Mathur, *J. Heat Transfer* **125**, 904 (2003).
- [41] H. Xie, M. Hu, and H. Bao, *Appl. Phys. Lett.* **104**, 131906 (2014).
- [42] H. Xie, T. Ouyang, É. Germaneau, G. Qin, M. Hu, and H. Bao, *Phys. Rev. B* **93**, 075404 (2016).
- [43] H. Dong, Z. Fan, L. Shi, A. Harju, and T. Ala-Nissila, *Phys. Rev. B* **97**, 094305 (2018).
- [44] W. Ma, T. Miao, X. Zhang, M. Kohno, and Y. Takata, *J. Phys. Chem. C* **119**, 5152 (2015).
- [45] C. Jeong, R. Kim, M. Luisier, S. Datta, and M. Lundstrom, *J. Appl. Phys.* **107**, 023707 (2010).
- [46] W. Li, J. Carrete, N. A. Katcho, and N. Mingo, *Comput. Phys. Commun.* **185**, 1747 (2014).